


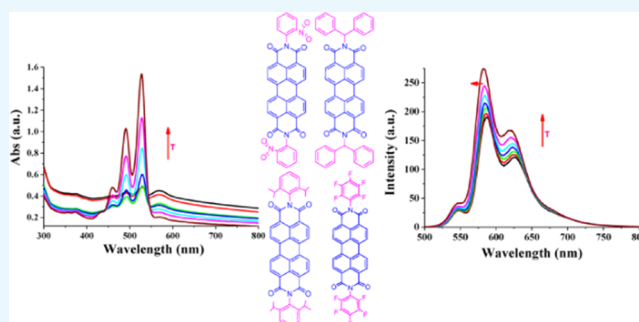
Facile Synthesis and Evaluation of Electron Transport and Photophysical Properties of Photoluminescent PDI Derivatives

Samya Naqvi,[†] Mahesh Kumar,[‡] and Rachana Kumar^{*,†} 

[†]Advanced Materials and Devices Metrology Division, Photovoltaic Metrology Group and [‡]Advanced Materials and Devices Metrology Division, Photonics Materials Metrology Group, CSIR-National Physical Laboratory, Dr. K. S. Krishnan Marg, New Delhi 110012, India

Supporting Information

ABSTRACT: Perylene-3,4,9,10-tetracarboxylic diimides (PDIs) have emerged as potential materials for optoelectronic applications. In the current work, four PDI derivatives, substituted at imide nitrogen with 2,6-diisopropyl phenyl, 2-nitrophenyl, diphenyl-methylene, and pentafluorophenyl groups, have been synthesized from perylene 3,4,9,10-tetracarboxylic dianhydride using a facile imidization synthesis process. PDI derivatives have been spectroscopically characterized for their structure and optical properties. Temperature-variable absorption and emission spectroscopy study confirmed the H-aggregation property. H-aggregation along with strong emission suggests the slipped π - π stacking of PDI molecules. Electrochemical analysis was performed for their redox behavior and calculation of lowest unoccupied molecular orbital and highest occupied molecular orbital energy levels. Scanning electron microscopy showed the formation of ordered structures. The PDI derivatives showed excellent electron conductivity without doping and 5–10 \times higher electron mobility than that of state-of-the-art fullerene acceptor phenyl-C₆₁-butyric acid methyl ester (PC₆₁BM). Finally, the charge generation and charge transfer phenomenon was studied by transient absorption spectroscopy (TAS). TAS showed ultrafast charge transfer from the poly(3-hexyl)thiophene (P3HT) donor polymer to PDI and formation of long-lived charge-separated states similar to fullerene derivative PC₆₁BM/P3HT blends. Such PDI derivatives with excellent solubility and photophysical and electronic properties are potential n-type materials to be used in organic electronic devices.



1. INTRODUCTION

Low-temperature solution-processable organic semiconductor materials are the requirement of current time for low-cost large-area fabrication of organic electronic devices on flexible substrates.¹ Compared to p-type organic semiconductor materials, n-type materials are relatively fewer and mainly focused on fullerene and its derivatives.² Rylene materials have got great attention in recent years, and several reports are available for their applications in organic electronic devices.³ Specially, perylene-3,4,9,10-tetracarboxylic diimides (PDIs) have shown their potential to be used in organic electronics.⁴ These molecules exhibit promising properties like strong light absorption, i.e., in the range of 400–450 nm (B band) and 500–700 nm (Q band)⁵ due to their extended conjugated π systems, self-assembling properties,⁶ low-lying frontier molecular orbitals, excellent electron mobility,⁷ high electron affinity, and photochemical and thermal stabilities.^{8,9} These molecules have been used for various applications like organic light emitting diodes,¹⁰ organic field effect transistors (OFETs),¹¹ organic solar cells,^{12–14} optical limiting¹⁵ and photochromic materials,¹⁶ etc. On the other hand, PDIs also possess some drawbacks like strong tendency of π - π stacking due to the planar structure resulting in limited solubility, poor fluorescence, and trapping of excitons in

organic solar cells.^{17,18} Charge carrier mobility is highly influenced by the morphology of materials and intermolecular interaction of molecules in films.¹⁹ There is need to synthesize PDI derivatives to generate photoluminescent (PL) charge transfer (CT) excitons. Therefore, to overcome these drawbacks, various groups are working through molecular designing, resulting in photoluminescent aggregates with facilitated charge transport and also developing new routes for the fabrication of air-stable organic devices.^{20–24}

The properties of PDIs have been tuned by modification of the substituents at imide nitrogen and bay positions. The substitution at imide nitrogen with strong electron-withdrawing groups shows little effect on optical and electronic properties but affects solubility. However, bay substituents affect electronic and optical properties, resulting in alteration of photophysical properties.^{25,26} In 2007, Marder and co-workers synthesized the first conjugated polymer-acceptor having the bay-substituted PDI with alternating dithienothiophene and PDI units exhibiting high electron mobility $\sim 1.3 \times 10^{-2} \text{ cm}^2 \text{ V}^{-1} \text{ s}^{-1}$

Received: August 6, 2019

Accepted: October 30, 2019

Published: November 12, 2019

and high electron affinity with a lowest unoccupied molecular orbital (LUMO) energy level of -3.9 eV.²⁷ The charge carrier mobility for this molecule was characterized in OFET geometry. Absorption and photoluminescence spectroscopy techniques have been used as the main tool to study the PDI aggregation behavior. There is still lack of complete characterization and analysis of substituents' effect on electrical and photophysical properties in neat as well donor/PDI blends. There are only a few reports on the study of PDI/donor mixtures for charge separation dynamics.²⁸ Recently, Tamai and co-workers reported the time evolution of electroabsorption caused by the electric field generated within electron–hole pairs using transient absorption spectroscopy (TAS) in a polymer solar cell with a perylene diimide (PDI) dimer acceptor.²⁹ From the study, they found that the charge carriers were generated very efficiently, i.e., $\sim 90\%$ of quantum yield, and separated within < 1 ps.

To expand the scope of PDI materials for efficient charge generation and charge separation and transport, the present work describes the synthesis and characterization of four PDI derivatives having a strong electron acceptor core substituted with different amine groups at the imide N position (Figure 1).

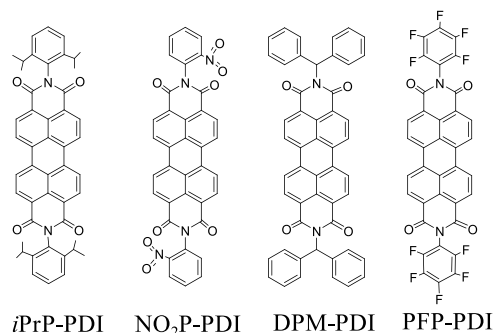


Figure 1. Chemical structures of synthesized PDI derivatives.

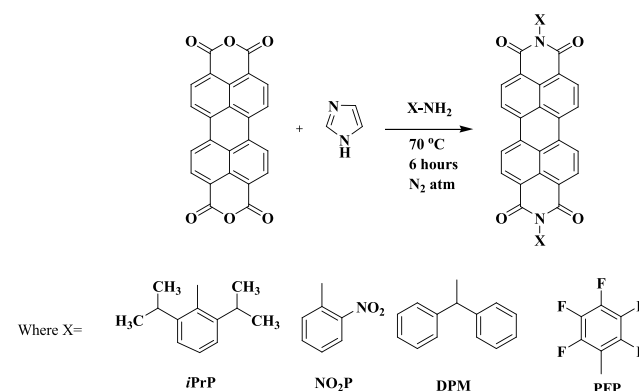
We have chosen two electron-donating [isopropylphenyl (*i*PrP) and diphenylmethylene (DPM)] substituents and two electron-withdrawing [nitrophenyl ((NO₂P)) and pentafluorophenyl (PFP)] substituents on the N-position and performed a comprehensive study of photophysical, electrochemical, and electron transport properties. These photoluminescent PDI derivatives form well-defined self-assembly, resulting in excellent optical and electrical properties. Electrical conductivity measurements were performed at different temperatures to study the effect of temperature on electrical current. The charge transport measurements of PDI derivatives were evaluated by the standard space charge limited current (SCLC) model and compared with the state-of-the-art fullerene acceptor phenyl-C₆₁-butyric acid methyl ester (PC₆₁BM). Transient absorption spectroscopy (TAS) ascertained ultrafast charge separation and formation of long-lived charge-separated states in these PDI derivatives on mixing with donor polymer poly(3-hexyl)-thiophene (P3HT).

2. RESULTS AND DISCUSSION

In the present work, we have synthesized four n-type perylene diimide (PDI) derivatives using a straightforward single-step reaction. The products were isolated as red solid materials and showed good solubility in chloroform and toluene (Scheme 1).

The structure of PDI derivatives was confirmed by Fourier transform infrared (FTIR) and ¹H NMR spectroscopy

Scheme 1. General Synthesis Scheme of PDI Derivatives



techniques. The parent material perylene 3,4,9,10-tetracarboxylic dianhydride (PTCDA) showed well-defined stretching peaks of dianhydride C=O at 1778 and 1761 cm^{-1} along with the aromatic C–H stretching peak at 3080 and aromatic C=C stretching peak at 1581 cm^{-1} (Figure S1).³⁰ On reaction with amines, substitution of anhydride oxygen with amine nitrogen takes place with formation of imide. To assure the formation of diimide without any impurity of monoimide, we performed FTIR spectroscopy of products and compared with that of precursor PTCDA. Anhydride carbonyl peaks completely disappeared in products with appearance of new intense peaks of C=O stretching (Figures S2 and S3). The other peaks of PTCDA, viz. 3035 (m, Ar–H) and 1592 (m, Ar C=C) cm^{-1} were retained in all of the products.

¹H NMR further confirmed the formation and purity of PDI derivatives and showed all of the alkyl and aromatic proton peaks. In *i*PrP-PDI, aromatic and aliphatic protons were clearly observed (Figure S4A). Eight aromatic protons of the PDI core appeared at 8.66 ppm. Six protons of the phenyl ring appeared at 7.38 and 7.13 ppm. Moreover, 24 methyl protons of the diisopropyl group were observed at 1.2 ppm and the peaks of four methanetriyl protons were clearly seen at 2.6 ppm. The molecular ion peak of *i*PrP-PDI appearing at m/z 711.3178 in the mass spectrum (Figure S4B) confirmed the formation of the desired product. For NO₂P-PDI, eight aromatic protons of the PDI core and eight phenyl protons of the nitrophenyl group were clearly seen at 8.67 ppm and at 7.28 and 7.45 ppm, respectively (Figure S5A). The molecular ion peak of NO₂P-PDI was observed at m/z 633.1704 (Figure S5B). For DPM-PDI, the 22 aromatic protons of the diphenylmethylene group appeared between 6.9 and 7.4 ppm and eight aromatic protons of the PDI core were observed at 8.67 ppm (Figure S6A). The m/z peak of DPM-PDI appeared at m/z 722.1506 (Figure S6B). ¹H NMR spectra of PFP-PDI showed the eight aromatic protons of the PDI core between 8.58 and 8.9 ppm (Figure S7A). The molecular ion peak of PFP-PDI was observed at m/z 722.0728 (Figure S7B).

2.1. Steady-State Absorption and Photoluminescence (PL) study. UV–visible absorption and photoluminescence study has been performed to characterize optical properties of PDI derivatives in solutions and in films. In dilute chloroform solution (0.01 mM), all of the PDIs showed distinct absorption bands at ~ 450 , 490, and 520 (Figure 2A and Table 1) for π – π^* electronic transitions, namely, 0–2, 0–1, and 0–0, respectively, for monomeric PDI chromophores in agreement with the literature for other perylenediimides³¹ and the Franck–Condon factor is in the order $A_{(0-0)} > A_{(0-1)} > A_{(0-2)}$.³²

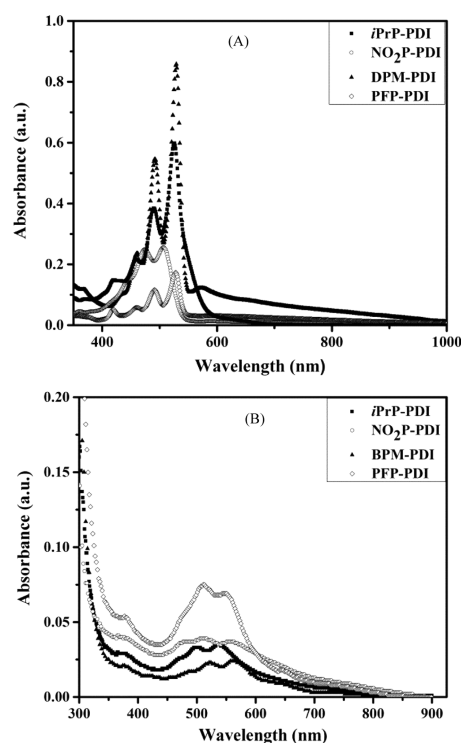


Figure 2. UV–visible absorption spectra of *iPrP*-PDI, NO_2P -PDI, DPM-PDI, and PFP-PDI in (A) chloroform (0.01 mM) solution and (B) spin-coated films.

The substituents on PDIs cause changes in relative absorbance of 0–1/0–0 absorption bands.³³ The relative intensity for the 0–1/0–0 transition was found to be 65, 98, 65, and 67% for *iPrP*-PDI, NO_2P -PDI, DPM-PDI, and PFP-PDI, respectively, indicating high probability of free PDI 0–0 transition in all of the cases except NO_2P -PDI. The nitrophenyl substituent causes enhanced 0–1 transition compared to other substituents, which may be due to different packing conformation in molecular self-assembly³⁴ (also discussed in Section 2.5), resulting in a mixture of monomeric and aggregated molecules. DPM-PDI shows additional absorption due to charge transfer (CT) exciton at 572 nm as also observed by Würthner et al., for an aryl-substituted PDI derivative in solution.³⁵ Absorption spectra were also recorded in films and show significantly broader absorption extended up to 800 nm (Figure 2B). A bathochromic shift was observed in films compared to solution (Table 1) as also observed for *N,N'*-bis(phenyl) PDI aggregates due to long-range Coulombic coupling.³⁶ Also, the relative absorbance of 0–1/0–0 bands was increased (94, 105, 93, and 108% for the four PDIs, respectively) due to aggregate formation.

PDI derivatives were further characterized for their fluorescence properties in solution and films as fluorescence is sensitive to the aggregation behavior of PDI. All of the PDI

derivatives showed distinct emission bands at ~ 550 , 580, and 620 nm for 0–0, 1–0, and 2–0 transitions, respectively, in solution (Figure 3A). Small Stokes shifts were observed for all of

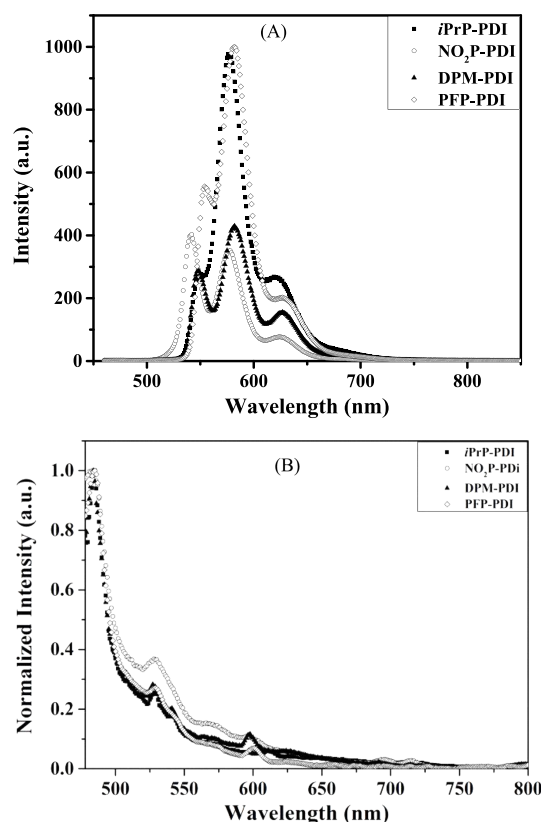


Figure 3. Fluorescence emission spectra of PDI derivatives in (A) chloroform solution and (B) spin-coated films on excitation with 450 nm.

the PDIs, indicating structural rigidity (Table 1). Appearance of high emission intensity suggests monomeric nature of PDI molecules in solution.³⁷ In films, distinct emission bands for 0–0, 1–0, and 2–0 transitions appeared at ~ 483 , 528, and 540 nm, respectively (Figure 3B). Excimer emission was observed in all of the four PDI films between ~ 600 and 750 nm as also observed by Chen et al., for fluorescent triarylphenyl-group-bearing PDI film due to face-to-face stacked dye aggregates.³⁸

We performed the concentration-variable absorption study in toluene to analyze the aggregate formation in detail.³⁹ Chloroform is the preferred solvent, and no aggregation was observed for PDI on increasing concentration; therefore, we chose toluene, a low-polarity solvent, to study the concentration effect on absorption. No shift was observed for band position with an increase in concentration; however, all of the PDIs showed change in absorbance. As can be seen in Figure S8, absorption due to the 0–1 vibronic transition in *iPrP*-PDI

Table 1. Absorption and Emission Data of PDI Derivatives in Chloroform Solution (0.01 M) and in Film

	abs. (solution) λ (nm)	abs. (film) λ (nm)	bathochromic shift (nm)	emission (solution) λ (nm)	emission (film) λ (nm)	Stokes shift (solution) (nm)
<i>iPrP</i> -PDI	459, 490, 529	471, 502, 538	~ 10	550, 576, 621	485, 529, 543, 612	25
NO_2P -PDI	440, 474, 507	477, 513, 560	~ 40	543, 577, 627	483, 529, 571, 597	36
DPM-PDI	460, 490, 529	487, 522, 559	~ 30	547, 584, 627	484, 527, 541, 589	18
PFP-PDI	458, 490, 528	473, 512, 548	~ 20	553, 582, 628	484, 528, 543, 600	25

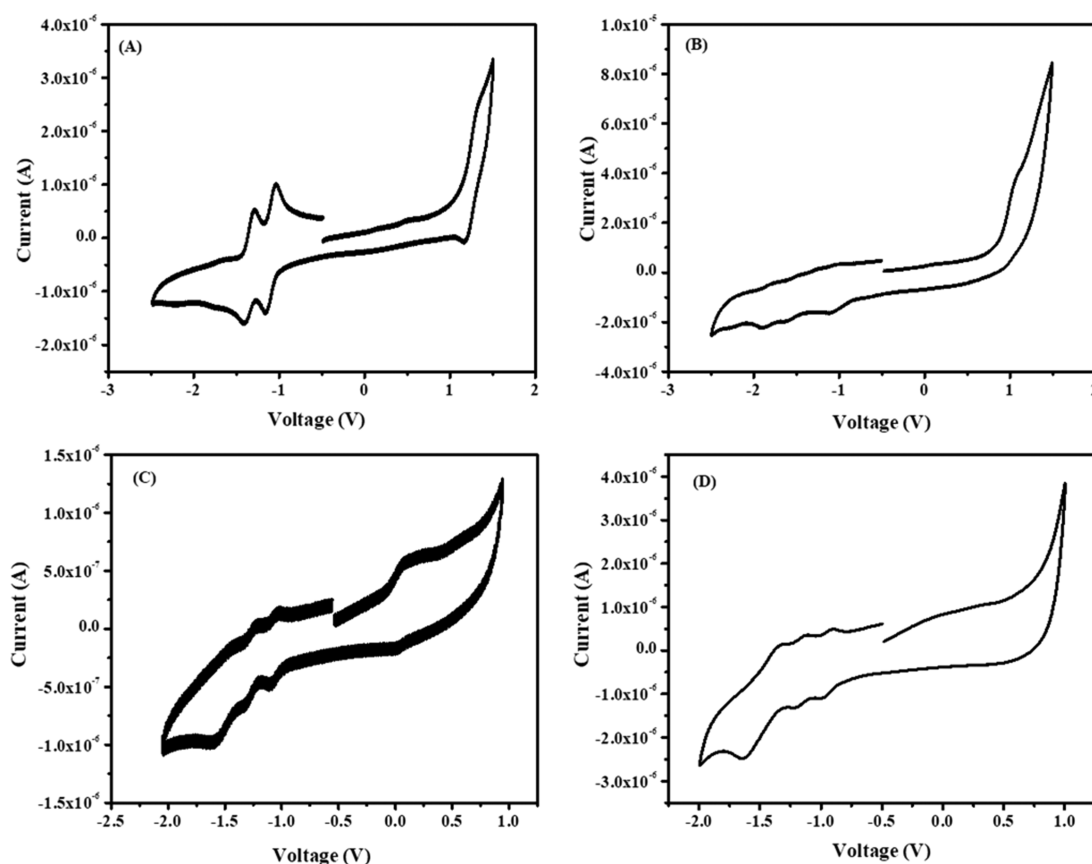


Figure 4. CV curves of (A) *i*PrP-PDI, (B) NO₂P-PDI, (C) DPM-PDI, and (D) PFP-PDI in *o*-dichlorobenzene (vs Fc/Fc⁺) with 0.1 M *n*-Bu₄NPF₆ as a supporting electrolyte with a scan rate of 50 mV s⁻¹.

increases with increasing concentration from 5 μ M to 0.5 mM. All vibronic features are lost in 0.5 mM solution, indicating electronic coupling between the molecules resulting in high aggregation.⁴⁰ For NO₂P-PDI also, 0–1 transition absorbance increases and reaches 0–0 transition absorbance but still is well defined. Interestingly, in DPM-PDI, absorbance at 575 nm increases and becomes equal to 0–0 transition absorbance at 0.5 mM concentration. This suggests aggregate formation with arrangement of molecule to effectively enhance the charge transfer between the perylene core and diphenylmethylene moiety. For PFP-PDI, we do not observe any effect of concentration increase on the absorption band structure and the relative intensity for the 0–1/0–0 transition is also maintained, indicating no significant ground state interaction between the PDI core of PFP-PDI molecules even at high concentration. Finally, we performed the analysis of the ratio of 0–1 vibronic transition absorbance to 0–0 vibronic transition absorbance $\{A_{(0-1)}/A_{(0-0)}\}$ with variation of concentration. This analysis allows us to identify the proximity of PDI molecules in solution. As reported by Wang et al.,⁴¹ a larger $A_{(0-1)}/A_{(0-0)}$ ratio promotes aggregate formation compared to lower $A_{(0-1)}/A_{(0-0)}$. They also observed the increase of the $A_{(0-1)}/A_{(0-0)}$ ratio with the concentration increase due to increased aggregation. In the present study also, there is increase in the $A_{(0-1)}/A_{(0-0)}$ ratio on increasing the concentration. However, in any case, 0–1 transition absorbance is not higher than that of the 0–0 transition ($A_{(0-1)}/A_{(0-0)}$ ratio ≤ 1). The exact face-to-face stacked H-aggregation results in 0–1 transition absorbance higher than that of the 0–0 transition.⁴² This observation suggests that the four PDIs have slipped face-to-face H-

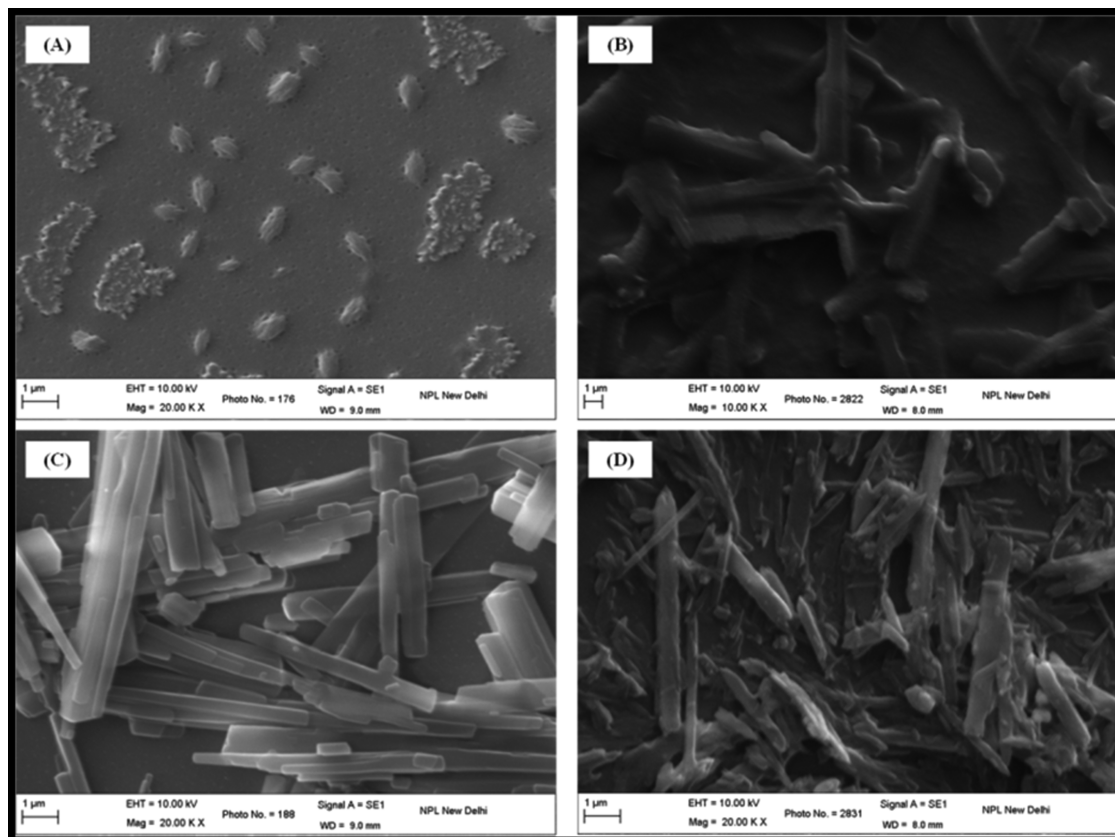
aggregation. PFP-PDI and DPM-PDI show least aggregate formation (Figure S9) and the $A_{(0-1)}/A_{(0-0)}$ ratio remains below 80% up to 0.5 mM concentration. However, *i*PrP-PDI and NO₂P-PDI show high aggregate formation above 50 μ M concentration of the solution as also discussed above.

Temperature-variable absorbance (40 μ M toluene solution) and photoluminescence (0.5 mM toluene solution) experiments were performed in toluene solution. The temperature was varied from 20 to 80 $^{\circ}$ C. Except PFP-PDI, all of the PDIs showed increase in absorbance on increasing the temperature along with a blue shift (Figure S11). The increase in absorbance with temperature indicates the presence of aggregates at low temperature, which convert into monomers on raising the temperature. PFP-PDI showed a decrease in absorbance with an increase in temperature, and the rationale could be temperature-induced disruption of molecular stacking. As observed earlier, no effect of increasing concentration on PFP-PDI supports the assumption. The temperature-variable emission study also showed intensity enhancement with a blue shift, indicating H-type aggregation (Figure S12). It is interesting observation, as H-aggregated PDIs show very weak emission,^{35a,36c} while in the present case, the strong photoluminescence with H-aggregation indicates rotationally displaced π – π stacked PDI molecules and needs theoretical support, which is beyond the scope of the current paper. Based on the absorption and photoluminescence study, we anticipate good electron conductivity and mobility in these PDI molecules due to effective π – π stacking and charge generation as discussed in later sections.

2.2. Electrochemical Analysis. The electrochemical properties of the products were measured by cyclic voltammetry

Table 2. Summarized Electrochemical Data of PDIs

	red _{onset} (V)	red ⁻¹	red ⁻²	red ⁻³	LUMO	optical band gap (eV)	HOMO
iPrP-PDI	-1.03	-1.18	-1.40		-3.77	2.1	-5.87
NO ₂ P-PDI	-0.96	-1.13	-1.63	-1.85	-3.84	2.27	-6.11
DPM-PDI	-1.08	-1.20	-1.44	-1.74	-3.72	2.23	-5.95
PPF-PDI	-0.88	-0.96	-1.22	-1.61	-3.92	2.25	-6.17

Figure 5. SEM spectra of (A) *iPrP*-PDI, (B) NO₂P-PDI, (C) DPM-PDI, and (D) PFP-PDI films.

(CV) to determine the oxidation and reduction potentials and energy levels. CV was performed in a three-electrode system, where a platinum disc was used as a working electrode, silver wire was used as a reference electrode, and platinum wire was used as a counter electrode. These CV plots were calibrated using the ferrocene/ferricenium couple as an internal reference to optimize the redox potentials. Reversible reduction potentials were observed for all of the PDIs as shown in Figure 4. The LUMO energy level of PDI derivatives was estimated from the onset reduction potential as summarized in Table 2. These values were measured from the empirical formula $E_{\text{HOMO/LUMO}} = -(E_{\text{onset}(\text{red/oxi})} + 4.8 \text{ eV})$ and are in accordance with the reported literature.⁴³ NO₂P-PDI and PFP-PDI having electron-withdrawing substituents show lower first reduction potential than *iPrP*-PDI and DPM-PDI. They also exhibit lower LUMO levels due to the presence of electron-withdrawing groups, suggesting stable anion formation and stability toward oxidation.⁴⁴ The band gap was calculated from the absorption edge and further used to calculate highest occupied molecular orbital (HOMO) energy levels (Table 2). PDIs with electron-donating groups show uplifted HOMO energy levels and lower band gaps due to the increased electron density. The energy levels and band gaps are in good agreement with previously reported data.⁴⁴

2.3. Self-Assembled Structures. The self-assembly of synthesized molecules into well-ordered one-dimensional supramolecular structures is highly dependent on the thermodynamic processes. Along with this, self-assembly of PDI derivatives is also highly dependent on the molecular stacking as well as on solubility.⁴⁵ The photophysical study in solution and films indicates strong π - π interactions between PDI molecules. It is important to observe their self-organizing behavior using the microscopy study; therefore, we performed scanning electron microscopy (SEM) analysis of casted films over a glass substrate using 0.5 mM toluene solution followed by annealing at 120 °C. The films were annealed to keep the same morphology as in the conductivity experiment and electron-only devices (Sections 2.4 and 2.5). As can be seen in Figure 5, *iPrP*-PDI shows globular structures, which may be due to distorted π - π stacking, preventing PDI molecules to assemble in one direction.^{34b} However, all other PDIs show tubular rod structures due to π - π stacking of PDI chromophore. The length of rods was in the range of few tens of microns and width \sim 500 nm as can be seen in Figure 5B–D. The SEM study further confirms the π - π stacking of PDI molecules with ordered structures as also concluded by the absorption and emission study.

2.4. Electrical Conductivity. We analyzed the electrical conductivity of PDI derivatives at different temperatures varying from 60 to 120 °C (Figure S14) for determining thermal-activated electrical conductivity. In our previous study, we have observed an increase in electrical conductivity with rise in temperature for HD-NDI materials without any additive.⁴⁶ Under dark testing conditions, a significant increase in electrical current was observed with an increase in voltage and so the conductivity (Figure S14). On the other hand, current also increases with an increase in test temperature, suggesting better stacking of PDI molecules, facilitating electron transport. A heating–cooling cycle was performed, and reversible performance was observed, indicating the robust structure of PDI derivatives under heating. Among the four PDIs, NO₂P-PDI showed the highest increase in current on increase in temperature and thus was most sensitive to temperature change. Such materials may find applications in temperature sensors.⁴⁷ This also supports the observation in Section 2.2, where NO₂P-PDI shows different behavior than other PDIs due to higher disorder. The highest conductivity of NO₂P-PDI and DPM-PDI observed at 100 °C was $\sim 5 \times 10^{-4}$ and 1×10^{-4} S m⁻¹, respectively, while *i*PrP-PDI and PFP-PDI showed highest conductivity of $\sim 0.64 \times 10^{-4}$ and 3.3×10^{-4} S m⁻¹, respectively, at 120 °C, which are very impressive among the rylene-diimides without additives.^{46,48} At high temperatures, the electron transport is facilitated by providing thermal energy to overcome the energy barrier due to disorders. In the present study also, the increase in temperature facilitates the electron transport as also observed earlier for symmetric columnar PDIs.⁴⁷

2.5. Electron Transport Studies. The electron mobility of all of the synthesized materials was investigated at variable thickness via standard electron-only device geometry as shown in Figure 6.^{46,49,50} The solution in chlorobenzene was prepared

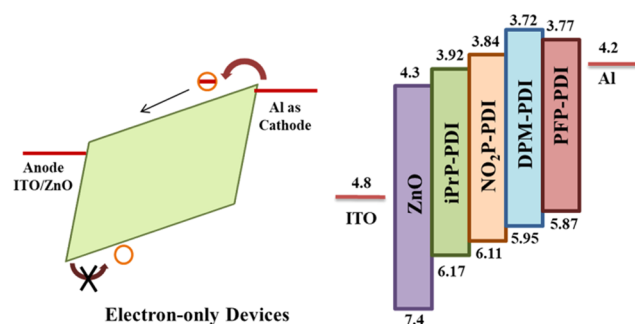


Figure 6. Schematic of the fabricated electron-only device with the energy level diagram of corresponding layers.

with different concentrations of 20, 30, and 40 mg/mL. A high boiling solvent is used to prepare solutions as the films are casted by spin-coating. A high boiling solvent like chlorobenzene evaporates slowly and forms continuous smooth film without pin holes. The PDI solution was spin-coated on top of the indium tin oxide (ITO)/ZnO substrate with annealing at 80 °C, and charge carrier mobility was determined from the SCLC model as shown in (Figure S15). By using the SCLC model, the current shows quadratic dependency on voltage at room temperature. With the help of the Mott–Gurney equation, electron mobility can be calculated

$$J = \frac{9}{8} \mu \epsilon \frac{V^2}{L^3}$$

Herein, J stands for the current density, μ is the mobility of the organic semiconductor, ϵ refers to the permittivity of medium, L is the thickness of the organic semiconductor layer, and V is the applied voltage.

Generally the charge carrier mobility in organic materials is low due to structural disorders in the films and decreases with decreasing film thickness. In the present work also, charge carrier mobility was found to decrease with decreasing active layer thickness. The calculated electron mobilities for PDI derivatives with variable thickness are summarized in Table 3. The highest

Table 3. Summarized Values of Electron Mobility for PDI Acceptors

thickness (nm)	mobility (cm ² V ⁻¹ s ⁻¹)			
	<i>i</i> PrA-PDI	NO ₂ A-PDI	BzHA-PDI	PFA-PDI
100	0.359×10^{-4}	3.84×10^{-5}	0.93×10^{-5}	0.53×10^{-5}
150	2.37×10^{-4}	1.51×10^{-4}	3.49×10^{-4}	4.55×10^{-5}
200	1.04×10^{-3}	0.58×10^{-3}	0.91×10^{-3}	0.50×10^{-3}

mobility values for all PDIs achieved with 200 nm thickness were 1.04×10^{-3} , 0.58×10^{-3} , 0.91×10^{-3} , and 0.504×10^{-3} cm² V⁻¹ s⁻¹ for *i*PrP-PDI, NO₂P-PDI, DPM-PDI, and PFP-PDI, respectively. The decreased film thickness mainly limits the charge carrier injection in the bulk of the material, which leads to the reduced carrier collection rate, resulting in decreased charge carrier mobility. However, all of the PDIs show comparable electron mobility to other reported PDIs (measured by the SCLC method).⁴³ Also, these PDIs show 5–10× higher mobility than that of the state-of-the-art fullerene acceptor PC₆₁BM (0.1×10^{-3} cm² V⁻¹ s⁻¹), making these PDIs potential acceptor materials for non-fullerene organic solar cells.⁵⁰

2.6. Transient Absorption Spectroscopy (TAS) Study.

Transient absorption spectroscopy has been performed to study the generation of charge-separated states in the donor/PDI blends for their future applications as acceptors in organic solar cells. We have chosen the most common donor polymer, i.e., P3HT. PDIs show formation of a singlet excited state after ~ 1 ps delay time between 650 and 950 nm, but no further transient species are observed in their TAS spectra due to very low efficiency of intersystem crossing.⁵¹ For the P3HT/PDI blend pump–probe measurement, 480 nm excitation wavelength was used to selectively excite P3HT molecules. Neat P3HT solution was used as a reference for determining the charge transfer mechanism in blends. The transient absorption spectra of P3HT (Figure S16) and mixture with different PDI derivatives in chloroform solution as a function of probe delay time have been shown in Figures 7 and 8. The transient absorption spectrum of P3HT below 2 ps showed strong stimulated emission (SE) at 580 and 625 nm. Transient absorption appears after 2 ps at ~ 1140 nm with a lifetime of 530 ps for the singlet excited state absorption of P3HT.⁵²

The transient absorption spectra of the P3HT mixture with PDI derivatives (equimolar) show completely different spectra than neat P3HT. In the P3HT/*i*PrP-PDI mixture, ground state absorption (GSA) bleaching due to PDI was observed at ~ 525 nm, while stimulated emission appeared at 575 and 625 nm (for the locally excited states) with lifetimes of 3.3 ns, 152 ps, and 390 ps, respectively (Figure 7A). After 1 ps of delay time, the strong transient absorption peak appears at 702 nm for the singlet excited state of the *i*PrP-PDI anion radical (PDI^{•-}) with a lifetime of 6 ns and disappearance of excited state emission.^{37,53}

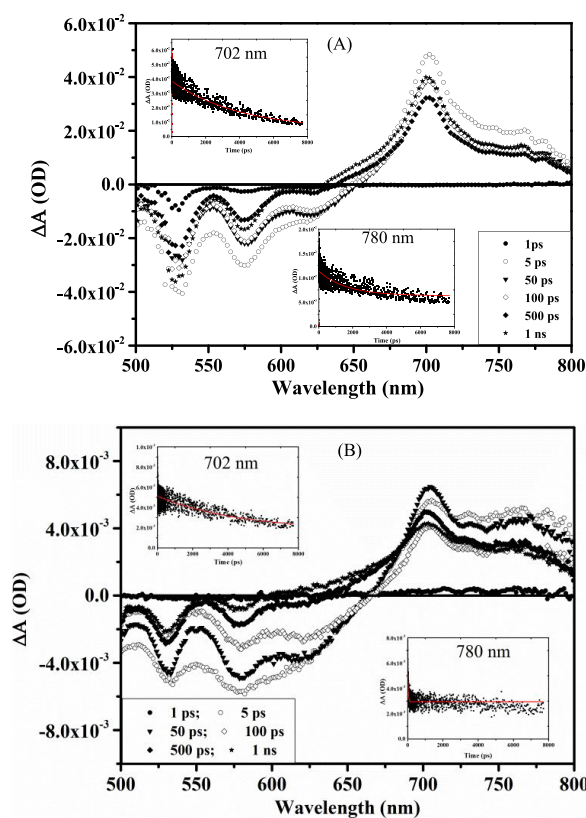


Figure 7. Transient absorption spectra of (A) *iPrP*-PDI and (B) NO_2P -PDI mixtures with P3HT in the UV–visible region on excitation with 480 nm wavelength.

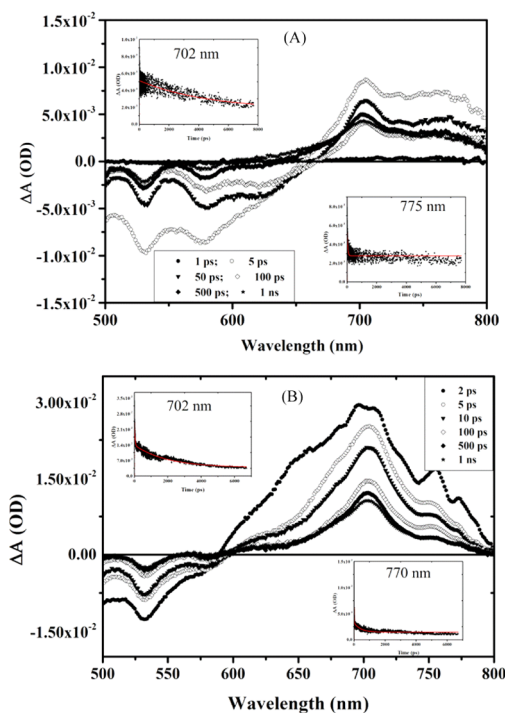


Figure 8. Transient absorption spectra of (A) DPM-PDI and (B) PFP-PDI mixtures with P3HT in the UV–visible region on excitation with 480 nm wavelength.

Transient absorption also appears between 750 and 800 nm with maxima at ~ 780 nm for the P3HT cation radical ($\text{P3HT}^{+\bullet}$) with

a lifetime of 1 ns. At the same time, the lifetime of the singlet excited state of P3HT at ~ 1140 nm was reduced to 172 ps in the mixture. Similar to *iPrP*-PDI, all other PDIs also showed GSA and SE after ~ 2 ps delay time. The stimulated emission was observed at 575 nm (219 ps), 630 nm (126 ps); 575 nm (214 ps), 630 nm (26 ps); and 575 nm (168 ps) (lifetime in parentheses) for NO_2P -PDI, DPM-PDI, and PFP-PDI respectively. There is subsequent loss of excited state emission with the appearance of excited state transient absorption in all of the cases.⁵³

All other P3HT/PDIs also show strong transient absorption for the P3HT cation radical between 750 and 800 nm, whereas the generation of PDI anion radical was observed at 705 nm (3 ns), 702 nm (3 ns), and 708 nm (1.77 ns) (lifetime in parentheses) for NO_2P -PDI, DPM-PDI, and PFP-PDI, respectively. Moreover, in all of the cases, the generation of charge-separated states, i.e., $\text{P3HT}^{+\bullet}$ and $\text{PDI}^{-\bullet}$, was observed at a very short delay time of ~ 2 ps and the lifetime of the P3HT singlet excited state of P3HT at ~ 1140 nm was reduced to 163, 167, and 38 ps for NO_2P -PDI, DPM-PDI, and PFP-PDI, respectively (Figure S17). This clearly indicates the electron transfer from the P3HT excited state to acceptor molecules, resulting in formation of charge-separated states with long lifetimes as seen in P3HT/methanofullerene blends.⁵³ The ultrafast charge transfer from the donor to acceptor favors the efficient charge carrier generation, and the long lifetime of the charge carriers reduces the recombination losses in solar cells. In the present study also, all of the PDIs show the generation of charge-separated states within few picoseconds with lifetime in nanoseconds.

Overall, the substituents on imide nitrogen influence the energy levels of PDI derivatives, and NO_2P -PDI and PFP-PDI showed uplifted LUMO levels, while *iPrP*-PDI and DPM-PDI showed uplifted HOMO levels. All of the PDIs showed similar photophysical and electronic properties. They showed monomeric nature in dilute solutions and H-type aggregation in the concentrated solution, resulting in defined structures as observed in SEM images. Ordered self-assembly of PDI derivatives resulted in good electrical conductivity without external doping and also showed moderate to high electron mobility. Finally, TAS clearly supported the efficient charge transfer interactions between PDI and P3HT polymer with generation of long-lived charge-separated states.

3. CONCLUSIONS

As a conclusion of the work, we have synthesized four different perylene diimide derivatives with substitution at the imide position via a simple synthesis process and studied their photophysical, self-assembling, and electronic properties. The study of vibronic peak strength for 0–1 and 0–0 transitions clearly suggests least aggregate formation in DPM-PDI and PFP-PDI, while *iPrP*-PDI and NO_2P -PDI are more prone to aggregation. The fluorescence measurement further suggests that although these PDIs form H-type aggregation, they still emit strongly in solution as well as in films. These materials also show excellent thermoactivated electron conductivity, and NO_2P -PDI can be used as a temperature sensor. The electron mobility of the materials was found to be 5–10 \times higher than that of PC_{61}BM . These observations indicate optimized molecular π – π stacking, resulting in strong fluorescence along with excellent electron transport. The charge-separated transient species (cation and anion radicals) in P3HT/PDI mixtures were observed at very short delay time (≤ 2 ps) with formation of long-lived charge-

separated states. The excellent electrical and optical properties of these materials make them a potential n-type material for wide applications in electronic devices.

4. EXPERIMENTAL SECTION

4.1. Materials and Characterization. Perylene-3,4,9,10 tetracarboxylic dianhydride (PTCDA) and aromatic amines, i.e., 2,6-diisopropylaniline, 2-nitroaniline, benzhydramine, and 2,3,4,5,6-pentafluoroaniline, were purchased from Sigma-Aldrich and used as received. All solvents were purchased from Alfa Aesar and used after drying. The reaction was carried out in an anhydrous solvent in oven-dried glassware under an inert environment of nitrogen. Silica gel thin-layer chromatography was used to monitor the progress of reaction, and the products were purified by column chromatography. Fourier transform infrared (FTIR) spectroscopy was done on PerkinElmer FTIR Spectrum 2. The sample was ground with anhydrous KBr, and pellets were prepared to record the spectrum from 4000 to 500 cm^{-1} . A background in air was done before recording data for samples. UV-vis absorption spectroscopy was performed on a Shimadzu UV-vis spectrophotometer (UV-1800) for solutions and spin-coated films. Products were also characterized for ^1H NMR on a Jeol 400 MHz spectrometer in deuterated chloroform (CDCl_3) using tetramethylsilane as the internal standard. We were not able to record ^{13}C NMR due to low concentration of products in solution. Matrix-assisted laser desorption ionization time-of-flight (MALDI-TOF)-TOF mass spectrometry AB SCIEX was used to determine the molecular weight of the products using α -cyano 4-hydroxy cinnamic acid matrix. The three-electrode standard configuration was used for cyclic voltammetry (CV) measurements using a platinum wire as the counter electrode, Ag wire as the reference electrode, and Pt disc as the working electrode in a 0.1 M tetra-*n*-butylammonium hexafluorophosphate in *o*-dichlorobenzene solution as electrolyte. Current vs voltage was measured on an Autolab potentiostat. Emission fluorescence measurements were performed on a Varian (CARY eclipse) fluorescence spectrophotometer in solution and also in films using 450 nm excitation wavelength. Thermal gravimetric analysis (TGA) was performed under 20 mL/min nitrogen flow using a PerkinElmer (Pyris 1) instrument, and loss in weight was recorded as a function of temperature. The samples were heated from room temperature to 700 $^\circ\text{C}$ at a ramp rate of 10 $^\circ\text{C}/\text{min}$. A Zeiss EVO-MA10 scanning electron microscope was used to analyze surface morphology and self-assembling properties of PDI derivatives. The samples were prepared by spin-coating 0.5 mM solution on cleaned glass substrates at 1000 rpm followed by annealing at 120 $^\circ\text{C}$. The electrical conductivities were measured at different temperatures by the two-probe method using bottom contact patterned ITO, applying high current source measurement and reading voltage change from a Keithley multimeter. Electron-only devices were fabricated as described earlier.^{46,49,50} Ultrafast transient absorption spectroscopy was performed using optical pulse from a Ti:sapphire laser amplifier (35 fs, 4 mJ/pulse, 1 kHz, 800 nm). A beam splitter was used to split the pulse into two beams. An optical parametric amplifier (TOPAS, Light Conversion) was employed on the high-intensity beam (pump) to vary the wavelength from 190 to 2600 nm. The weak-intensity beam (probe) was propagated through a CaF_2 crystal to generate white light continuum. A computer-controlled delay stage was used to optically delay the probe beam with respect to the pump beam. In the current study, we used 480 nm wavelength as a pump beam at normal

incidence, and the changes in absorption were detected using a gated CMOS detector. The time-resolved study was performed using a HELIOS (Ultrafast Systems) spectrometer.

4.2. Synthesis of PDI Derivatives (Scheme 1). **4.2.1. Synthesis of *iPrP*-PDI.** Perylene-3,4,9,10 tetracarboxylic dianhydride (500 mg, 1.23 mM), 2,6-diisopropylaniline (1.22 mL, 6.5025 mM), and imidazole (3 g, 0.044 mM) were added to a degassed 100 mL two-neck round-bottom flask. The reaction mixture was stirred at 120 $^\circ\text{C}$ for 6 h under a nitrogen atmosphere. The reaction mixture was cooled to room temperature and poured into 100 mL of distilled water. The precipitate was filtered using a Buckner funnel and washed with distilled water followed by drying under vacuum at 50 $^\circ\text{C}$. The dried material was purified by column chromatography using an 18 mm diameter and 250 mm long column packed with 100 mesh silica gel. The chloroform/hexane (80:20) mixture was used as eluent. The pure product obtained was deep red, as a second band.

iPrP-PDI: Yield: \sim 60%; FTIR (ν , cm^{-1}): 2985 (m, Ar C–H), 2934 (m, C–H), 1714 (s, C=O), 1654 (s, C=O), 1599 (s, C=C), 1464 (s, C–H); ^1H NMR (CDCl_3 , 400 MHz), δ (ppm): 1.2 (m, 24H), 2.6 (br, 4H), 7.1 (m, 2H), 7.3 (m, 4H), 8.6 (m, 8H); high-resolution mass spectrometry (HRMS) (MALDI-TOF) for formula $\text{C}_{48}\text{H}_{42}\text{N}_2\text{O}_4$ calcd 710.3145 experimental mass ($M + 1$) (m/z): 711.3178.

4.2.2. Synthesis of *NO₂P*-PDI. Perylene-3,4,9,10 tetracarboxylic dianhydride (500 mg, 1.23 mM), 2-nitroaniline (897 mg, 6.5025 mM), imidazole (3 g, 0.044 mM) were added to a degassed 100 mL two-neck round-bottom flask. Thereafter, the reaction mixture was refluxed with continuous stirring at 120 $^\circ\text{C}$ for 6 h under a nitrogen atmosphere. Precipitation was done by adding 100 mL of distilled water into the reaction mixture. The crude product was collected by filtration and washed several times with distilled water followed by purification with column chromatography (18 mm \times 200 mm) on silica gel using chloroform as eluent. In the column, two fractions were collected, and the second fraction was the desired product. After evaporation of the solvent, the solid product was obtained from fraction 2.

NO₂P-PDI: Yield: \sim 20%; FTIR (ν , cm^{-1}): 3028 (w, Ar C–H), 1713 (m, C=O), 1670 (s, C=O), 1595 (s, C=C), 1511 (s, N–O); ^1H NMR (CDCl_3 , 400 MHz), δ (ppm): 7.28 (m, 4H), 7.45 (m, 4H), 8.673 (m, 8H). HRMS (MALDI-TOF) for formula $\text{C}_{36}\text{H}_{16}\text{N}_4\text{O}_8$ calcd 632.0968 experimental mass ($M + 1$) (m/z): 633.1704.

4.2.3. Synthesis of *DPM*-PDI. Perylene-3,4,9,10 tetracarboxylic dianhydride (300 mg, 0.7908 mM), benzhydramine (0.562 mL, 3.1632 mM), and imidazole (3 g, 0.044 mM) were added to a degassed two-neck round-bottom flask. Then, the reaction mixture was refluxed at 110 $^\circ\text{C}$ for 6 h with regular stirring under a nitrogen atmosphere. The reaction mixture was cooled to room temperature and precipitated by adding 100 mL of distilled water followed by filtration. Purification was done by column chromatography (18 mm \times 200 mm), and the second fraction obtained was the desired product.

DPM-PDI: Yield: \sim 70%; FTIR (ν , cm^{-1}): 3023 (w, Ar C–H), 2905 (m, C–H), 1703 (s, C=O), 1659 (s, C=O), 1592 (s, C=C), 1496 (s, C–H); ^1H NMR (CDCl_3 , 400 MHz), δ (ppm): 6.94 (s, 2H), 7.3 (m, 8H), 7.42 (m, 12 H), 8.673 (m, 8H). HRMS (MALDI-TOF) for formula $\text{C}_{50}\text{H}_{30}\text{N}_2\text{O}_4$ calcd 722.2206 experimental mass (M) (m/z): 722.1506.

4.2.4. Synthesis of *PFP*-PDI. Perylene-3,4,9,10 tetracarboxylic dianhydride (300 mg, 0.76 mM), 2,3,4,5,6-pentafluoroaniline

(559 mg, 3.06 mM), and imidazole (3 g, 0.044 mM) were added to a two-neck round-bottom flask followed by regular nitrogen purging. The reaction mixture was refluxed with stirring for 6 h and poured into 100 mL of distilled water, and the precipitate was collected by filtration and then dried under vacuum. The solvent was removed using rotavapor, and the fluorescent red compound was isolated by column chromatography (18 mm × 250 mm) using chloroform as eluent.

PFP-PDI: Yield: ~60%; FTIR (ν , cm^{-1}) 3098 (w, Ar C–H), 1720 (s, C=O), 1682 (s, C=O), 1594 (s, C=C); 1525, 1506 (s, =C–F); ^1H NMR (CDCl_3 , 400 MHz), δ (ppm): 8.58 (m, 4H), 8.9 (m, 4H). HRMS (MALDI-TOF) for formula $\text{C}_{36}\text{H}_8\text{F}_{10}\text{N}_2\text{O}_4$ calcd 722.0324 experimental mass (M) (m/z): 722.0728.

■ ASSOCIATED CONTENT

Supporting Information

The Supporting Information is available free of charge on the ACS Publications website at DOI: [10.1021/acsomega.9b02514](https://doi.org/10.1021/acsomega.9b02514).

FTIR spectra of PTCDA (Figure S1), iPrP-PDI and NO_2P -PDI (Figure S2), and DPM-PDI and PFP-PDI (Figure S3); ^1H NMR and HRMS spectra PDIs (Figures S4–S7); concentration-variable absorption spectra of PDIs (Figure S8); comparative $A_{(0-1)}/A_{(0-0)}$ transition with change in concentration (Figure S9); comparative absorption emission spectra of the PDIs (Figure S10); temperature-variable (20–80 °C) absorption and fluorescence spectra of PDI derivatives in toluene solution (Figures S11 and S12); TGA under N_2 flow of 20 mL min^{-1} at 10 °C min^{-1} temperature ramping (Figure S13); electrical conductivity data (Figure S14); electron transport J – V plots for all of the four PDIs (Figure S15); P3HT TAS spectra (Figure S16); and TAS spectra of the P3HT mixture (Figure S17) (PDF)

■ AUTHOR INFORMATION

Corresponding Author

*E-mail: rachanak.npl@nic.in, rachanasinghchem@gmail.com.
Tel: +91-11-4560-8577. Fax: +91-11-4560-9310.

ORCID

Rachana Kumar: 0000-0002-7567-7775

Notes

The authors declare no competing financial interest.

■ REFERENCES

(1) (a) Kim, J. J.; Han, M. K.; Noh, Y. Y. Flexible OLEDs and organic electronics. *Semicond. Sci. Technol.* **2011**, *26*, No. 030301. (b) Kelley, T. W.; Baude, P. F.; Gerlach, C.; Ender, D. E.; Muyres, D.; Haase, M. A.; Vogel, S. E.; Theiss, S. D. Recent Progress in Organic Electronics: Materials, Devices, and Processes. *Chem. Mater.* **2004**, *16*, 4413–4422. (c) Krieg, E.; Elkan, A. N.; Cohen, E.; Tsarfati, Y.; Rybtchinski, B. Noncovalent aqua materials based on perylene diimides. *Acc. Chem. Res.* **2019**, *52*, 2634–2646.
(2) (a) Umeyama, T.; Imahori, H. Isomer Effects of Fullerene Derivatives on Organic Photovoltaics and Perovskite Solar Cells. *Acc. Chem. Res.* **2019**, *52*, 2046–2055. (b) Quinn, J. T. E.; Zhu, J.; Li, X.; Wang, J.; Li, Y. Recent progress in the development of n-type organic semiconductors for organic field effect transistors. *J. Mater. Chem. C* **2017**, *5*, 8654–8681. (c) Ando, S.; Nishida, J.; Fujiwara, E.; Tada, H.; Inoue, Y.; Tokito, S.; Yamashita, Y. Novel p- and n-Type Organic Semiconductors with an Anthracene Unit. *Chem. Mater.* **2005**, *17*, 1261–1264.

(3) Yan, C.; Barlow, S.; Wang, Z.; Yan, H.; Jen, A. K. Y.; Marder, S. R.; Zhan, X. Non-fullerene acceptors for organic solar cells. *Nat. Rev.* **2018**, *3*, No. 18003.

(4) (a) Huang, C.; Barlow, S.; Marder, S. R. Perylene-3,4,9,10-tetracarboxylic Acid Diimides: Synthesis, Physical Properties, and Use in Organic Electronics. *J. Org. Chem.* **2011**, *76*, 2386–2407. (b) Sharenko, A.; Proctor, C. M.; Van der Poll, T. S.; Henson, Z. B.; Nguyen, T. Q.; Bazan, G. C. A high-performing solution processed small molecule:perylene diimide bulk heterojunction solar cell. *Adv. Mater.* **2013**, *25*, 4403–4406. (c) Hartnett, P. E.; Timalsina, A.; Matte, H. S. S. R.; Zhou, N.; Guo, X.; Zhao, W.; Facchetti, A.; Chang, R. P. H.; Hersam, M. C.; Wasielewski, M. R.; Marks, T. J. Slip-stacked perylenediimides as an alternative strategy for high efficiency nonfullerene acceptors in organic photovoltaics. *J. Am. Chem. Soc.* **2014**, *136*, 16345–16356. (d) Yang, X.; Zhao, Z.; Ran, H.; Zhang, J.; Chen, L.; Han, R.; Duan, X.; Sun, H.; Hu, J.-Y. New pyrene-based butterfly-shaped blue AIEgens: Synthesis, structure, aggregation-induced emission and their nondoped blue OLEDs. *Dyes Pigm.* **2019**, No. 107881.

(5) Dinçalp, H.; Çimen, O.; Ameri, T.; Brabec, C. J. Synthesis, characterization and optoelectronic properties of a new perylene diimide–benzimidazole type solar light harvesting dye. *Spectrochim. Acta, Part A* **2014**, *128*, 197–206.

(6) (a) You, C. C.; Würthner, F. Self-Assembly of Ferrocene-Functionalized Perylene Bisimide Bridging Ligands with Pt(II) Corner to Electrochemically Active Molecular Squares. *J. Am. Chem. Soc.* **2003**, *125*, 9716–9725. (b) Würthner, F.; Thalacker, C.; Sautter, A. Hierarchical Organization of Functional Perylene Chromophores to Mesoscopic Superstructures by Hydrogen Bonding and π – π Interactions. *Adv. Mater.* **1999**, *11*, 754–758. (c) van der Boom, T.; Hayes, R. T.; Zhao, Y.; Bushard, P. J.; Weiss, E. A.; Wasielewski, M. R. Charge Transport in Photofunctional Nanoparticles Self-Assembled from Zinc 5,10,15,20-Tetrakis(perylene-diimide)porphyrin Building Blocks. *J. Am. Chem. Soc.* **2002**, *124*, 9582–9590. (d) Dobrawa, R.; Würthner, F. Photoluminescent supramolecular polymers: metal-ion directed polymerization of terpyridine-functionalized perylene bisimide dyes. *Chem. Commun.* **2002**, 1878–1879.

(7) Liu, Y.; Wang, Y.; Ai, L.; Liu, Z.; Ouyang, X.; Ge, Z. Perylenebisimide regioisomers: Effect of substituent position on their spectroscopic, electrochemical, and photovoltaic properties. *Dyes Pigm.* **2015**, *121*, 363–371.

(8) Tahir, M.; Sayyad, M. H.; Wahab, F.; Aziz, F.; Shahid, M.; Munawar, M. A. Perylene diimide: Synthesis, fabrication and temperature dependent electrical characterization of heterojunction with p-silicon. *Phys. B* **2013**, *426*, 6–12.

(9) Mikroyannidis, J. A.; Stylianakis, M. M.; Sharma, G. D.; Balraju, P.; Roy, M. S. A Novel Alternating Phenylenevinylene Copolymer with Perylene Bisimide Units: Synthesis, Photophysical, Electrochemical, and Photovoltaic Properties. *J. Phys. Chem. C* **2009**, *113*, 7904–7912.

(10) Matsui, M.; Wang, M.; Funabiki, K.; Hayakawa, Y.; Kitaguchi, T. Properties of novel perylene-3,4,9,10-tetracarboxydiimide-centred dendrimers and their application as emitters in organic electroluminescence devices. *Dyes Pigm.* **2007**, *74*, 169–175.

(11) Würthner, F.; Stolte, M. Naphthalene and perylene diimides for organic transistors. *Chem. Commun.* **2011**, *47*, 5109–5115.

(12) Kozma, E.; Catellani, M. Perylene diimides based materials for organic solar cells. *Dyes Pigm.* **2013**, *98*, 160–179.

(13) Choi, H.; Paek, S.; Song, J.; Kim, C.; Cho, N.; Ko, J. Synthesis of annulated thiophene perylene bisimide analogues: their applications to bulk heterojunction organic solar cells. *Chem. Commun.* **2011**, *47*, 5509–5511.

(14) Hains, A. W.; Liang, Z.; Woodhouse, M. A.; Gregg, B. A. Molecular Semiconductors in Organic Photovoltaic Cells. *Chem. Rev.* **2010**, *110*, 6689–6735.

(15) Law, K. Y. Organic photoconductive materials: recent trends and developments. *Chem. Rev.* **1993**, *93*, 449–486.

(16) (a) Tan, W.; Li, X.; Zhang, J.; Tian, H. A photochromic diarylethene dyad based on perylene diimide. *Dyes Pigm.* **2011**, *89*, 260–265. (b) Würthner, F. Perylene bisimide dyes as versatile building

blocks for functional supramolecular architectures. *Chem. Commun.* **2004**, 1564–1579. (c) Kohl, C.; Weil, T.; Qu, J.; Müllen, K. Towards Highly Fluorescent and Water-Soluble Perylene Dyes. *Chem. – Eur. J.* **2004**, *10*, 5297–5310. (d) Margineanu, A.; Hofkens, J.; Cotlet, M.; Habuchi, S.; Stefan, A.; Qu, J.; Kohl, C. F.; Müllen, K.; Vercammen, J.; Engelborghs, Y.; Gensch, T.; De Schryver, F. C. Photophysics of a Water-Soluble Rylene Dye: Comparison with Other Fluorescent Molecules for Biological Applications. *J. Phys. Chem. B* **2004**, *108*, 12242–12251.

(17) Ahrens, M. J.; Tauber, M. J.; Wasielewski, M. R. Bis(*n*-octylamino)perylene-3,4:9,10-bis(dicarboximide)s and Their Radical Cations: Synthesis, Electrochemistry, and ENDOR Spectroscopy. *J. Org. Chem.* **2006**, *71*, 2107–2114.

(18) Handa, N. V.; Mendoza, K. D.; Shirtcliff, L. D. Synthesis and Properties of 1,6 and 1,7 Perylene Diimides and Tetracarboxylic Dianhydrides. *Org. Lett.* **2011**, *13*, 4724–4727.

(19) Guo, Y.; Han, G.; Yi, Y. Impact of alkyl chain branching positions on molecular packing and electron transport of dimeric perylene diimide derivatives. *J. Energy Chem.* **2019**, *35*, 138–143.

(20) (a) Langhals, H. Control of the Interactions in Multi-chromophores: Novel Concepts. Perylene Bis-imides as Components for Larger Functional Units. *Helv. Chim. Acta* **2005**, *88*, 1309–1343.

(b) Langhals, H.; Ismael, R.; Yürük, O. Persistent Fluorescence of Perylene Dyes by Steric Inhibition of Aggregation. *Tetrahedron* **2000**, *56*, 5435–5441. (c) Görl, D.; Zhang, X.; Würthner, F. Molecular Assemblies of Perylene Bisimide Dyes in Water. *Angew. Chem., Int. Ed.* **2012**, *51*, 6328–6348. (d) Weil, T.; Vosch, T.; Hofkens, J.; Peneva, K.; Müllen, K. The rylene colorant family–tailored nanoemitters for photonics research and applications. *Angew. Chem., Int. Ed.* **2010**, *49*, 9068–9093. (e) Montalti, M.; Battistelli, G.; Cantelli, A.; Genovese, D. Photo-tunable multicolour fluorescence imaging based on self-assembled fluorogenic nanoparticles. *Chem. Commun.* **2014**, *50*, 5326–5329. (f) Kaiser, T. E.; Wang, H.; Stepanenko, V.; Würthner, F. Supramolecular construction of fluorescent J-aggregates based on hydrogen-bonded perylene dyes. *Angew. Chem., Int. Ed.* **2007**, *46*, 5541–5544. (g) Zhang, X.; Chen, Z.; Würthner, F. Morphology Control of Fluorescent Nanoaggregates by Co-Self-Assembly of Wedge- and Dumbbell-Shaped Amphiphilic Perylene Bisimides. *J. Am. Chem. Soc.* **2007**, *129*, 4886–4887. (h) Yagai, S.; Seki, T.; Karatsu, T.; Kitamura, A.; Würthner, F. Transformation from H- to J-aggregated perylene bisimide dyes by complexation with cyanurates. *Angew. Chem., Int. Ed.* **2008**, *47*, 3367–3371.

(21) Balaji, G.; Kale, T. S.; Keerthi, A.; Pelle, A. M. D.; Thayumanavan, S.; Valiyaveetil, S. Low Band Gap Thiophene–Perylene Diimide Systems with Tunable Charge Transport Properties. *Org. Lett.* **2011**, *13*, 18–21.

(22) Rajaram, S.; Shivanna, R.; Kandappa, S.; Narayan, K. Nonplanar Perylene Diimides as Potential Alternatives to Fullerene in Organic Solar Cells. *J. Phys. Chem. Lett.* **2012**, *3*, 2405–2408.

(23) Chen, W.; Yang, X.; Long, G.; Wan, X.; Chen, Y.; Zhang, Q. A perylene diimide (PDI) based small molecule with tetrahedral configuration as a non-fullerene acceptor for organic solar cells. *J. Mater. Chem. C* **2015**, *3*, 4698–4705.

(24) Hartnett, P. E.; Matte, H. S. S.; Eastham, N. D.; Jackson, N. E.; Wu, Y.; Chen, L. X.; Ratner, M. A.; Chang, R. P. H.; Hersam, M. C.; Wasielewski, M. R.; Marks, T. J. Ring-fusion as a perylene diimide dimer design concept for high-performance non-fullerene organic photovoltaic acceptors. *Chem. Sci.* **2016**, *7*, 3543–3555.

(25) Huang, C.; Barlow, S.; Marder, S. R. Perylene-3,4,9,10-tetracarboxylic Acid Diimides: Synthesis, Physical Properties, and Use in Organic Electronics. *J. Org. Chem.* **2011**, *76*, 2386–2407.

(26) Zhao, H.; Zhang, Y.; Xu, H.; He, Z.; Zhang, Z.; Zhang, H. Synthesis and properties of perylene diimide dyes bearing unsymmetrical and symmetrical phenoxy substituents at bay positions. *Tetrahedron* **2015**, *71*, 7752–7757.

(27) Zhan, X.; Tan, Z.; Domercq, B.; An, Z.; Zhang, X.; Barlow, S.; Li, Y.; Zhu, D.; Kippelen, B.; Marder, S. R. A High-Mobility Electron-Transport Polymer with Broad Absorption and Its Use in Field-Effect

Transistors and All-Polymer Solar Cells. *J. Am. Chem. Soc.* **2007**, *129*, 7246–7247.

(28) (a) Ziffer, M. E.; Jo, S. B.; Zhong, H.; Ye, L.; Liu, H.; Lin, F.; Zhang, J.; Li, X.; Ade, H. W.; Jen, A. K.-Y.; Ginger, A. D. S. Long-Lived, Non-Geminate, Radiative Recombination of Photogenerated Charges in a Polymer/Small-Molecule Acceptor Photovoltaic Blend. *J. Am. Chem. Soc.* **2018**, *140*, 9996–10008. (b) Walwark, D. J., Jr.; Datko, B. D.; Wu, Q.; Neshchadin, A.; Berrens, M. L.; Yu, L.; Grey, J. K. Conformational Flexibility Determines Electronic Coupling and Charge Transfer Character in Single Propeller-Shaped Perylene Diimide Tetramer Arrays. *J. Phys. Chem. C* **2018**, *122*, 23261–23270.

(29) Tamai, Y.; Fan, Y.; Kim, V. O.; Ziabrev, K.; Rao, A.; Barlow, S.; Marder, S. R.; Friend, R. H.; Menke, S. M. Ultrafast Long-Range Charge Separation in Nonfullerene Organic Solar Cells. *ACS Nano* **2017**, *11*, 12473–12488.

(30) Chen, Y.; Qian, J.; Liu, X.; Zhuang, Q.; Han, Z. Synthesis and photoluminescence properties of polybenzoxazoles containing perylenebisimide functionalized graphene nanosheets via stacking interactions. *New J. Chem.* **2013**, *37*, 2500–2508.

(31) (a) Nakazono, S.; Imazaki, Y.; Yoo, H.; Yang, J.; Sasamori, T.; Tokitoh, N.; Cedric, T.; Kageyama, H.; Kim, D.; Shinokubo, H.; Osuka, A. Regioselective Ru-catalyzed direct 2,5,8,11-alkylation of perylene bisimides. *Chem. – Eur. J.* **2009**, *15*, 7530–7533. (b) Nakazono, S.; Easwaramoorthi, S.; Kim, D.; Shinokubo, H.; Osuka, A. Synthesis of arylated perylene bisimides through C-H bond cleavage under ruthenium catalysis. *Org. Lett.* **2009**, *11*, 5426–5429.

(32) Yan, Q.; Cai, K.; Zhao, D. Supramolecular aggregates with distinct optical properties from PDI oligomers of similar structures. *Phys. Chem. Chem. Phys.* **2016**, *18*, 1905–1910.

(33) Khan, Q. U.; Tian, G.; Bao, L.; Qi, S.; Wu, D. Highly uniform supramolecular nano-films derived from carbazole-containing perylene diimide via surface-supported self-assembly and their electrically bistable memory behaviour. *New J. Chem.* **2018**, *42*, 11506–11515.

(34) (a) Balakrishnan, K.; Datar, A.; Naddo, T.; Huang, J.; Oitker, R.; Yen, M.; Zhao, J.; Zang, L. Effect of Side-Chain Substituents on Self-Assembly of Perylene Diimide Molecules: Morphology Control. *J. Am. Chem. Soc.* **2006**, *128*, 7390–7398. (b) Pagoaga, B.; Mongin, O.; Caselli, M.; Vanossi, D.; Momichhioli, F.; Blanchard-Desce, M.; Lemerrier, G.; Hoffmann, N.; Ponterini, G. Optical and photophysical properties of anisole and cyanobenzene-substituted perylene diimides. *Phys. Chem. Chem. Phys.* **2016**, *18*, 4924–4941. (c) Klebe, G.; Graser, F.; Hadicke, E.; Berndt, J. Crystallochromy as a solid-state effect: correlation of molecular conformation, crystal packing and colour in perylene-3,4:9,10-bis-(dicarboximide) pigments. *Acta Crystallogr., Sect. B: Struct. Sci.* **1989**, *45*, 69–77. (d) Kazmaier, P. M.; Hoffmann, R. A Theoretical Study of Crystallochromy. Quantum Interference Effects in the Spectra of Perylene Pigments. *J. Am. Chem. Soc.* **1994**, *116*, 9684–9691.

(35) (a) Würthner, F.; Chen, Z.; Delm, V.; Stepanenko, V. One-dimensional luminescent nanoaggregates of perylene bisimides. *Chem. Commun.* **2006**, 1188–1190. (b) Forrst, S. R. Ultrathin Organic Films Grown by Organic Molecular Beam Deposition and Related Techniques. *Chem. Rev.* **1997**, *97*, 1793–1896.

(36) (a) Hestand, N. J.; Spano, F. C. Expanded Theory of H- and J-Molecular Aggregates: The Effects of Vibronic Coupling and Intermolecular Charge Transfer. *Chem. Rev.* **2018**, *118*, 7069–7163. (b) Zhao, D.; Wu, Q.; Cai, Z.; Zheng, T.; Chen, W.; Lu, J.; Yu, L. Electron acceptors based on alpha-substituted PDI for organic solar cells. *Chem. Mater.* **2016**, *28*, 1139–1146. (c) Oleson, A.; Zhu, T.; Dunn, I. S.; Bialas, D.; Bai, Y.; Zhang, W.; Dai, M.; Reichman, D. R.; Tempelaar, R.; Huang, L.; Spano, F. C. Perylene Diimide-Based H_j- and h_j-Aggregates: The Prospect of Exciton Band Shape Engineering in Organic Materials. *J. Phys. Chem. C* **2019**, *123*, 20567–20578.

(37) Clark, A. E.; Qin, C.; Li, A. D. Beyond Exciton Theory: A Time-Dependent DFT and Franck–Condon Study of Perylene Diimide and Its Chromophoric Dimer. *J. Am. Chem. Soc.* **2007**, *129*, 7586–7595.

(38) (a) Chen, Z.; Stepanenko, V.; Dehm, V.; Prins, P.; Siebbeles, L. D. A.; Seibt, J.; Marquetand, P.; Engel, V.; Würthner, F. High Excimer-State Emission of Perylene Bisimides and Recognition of Latent

Fingerprints. *Chem. – Eur. J.* **2007**, *13*, 436–449. (b) Refiker, H.; Icil, H. Amphiphilic and chiral unsymmetrical perylene dye for solid-state dye-sensitized solar cells. *Turk. J. Chem.* **2011**, *35*, 847–859.

(39) (a) Würthner, F.; Saha-Möller, C. R.; Fimmel, B.; Ogi, S.; Leowanawat, P.; Schmidt, D. Perylene Bisimide Dye Assemblies as Archetype Functional Supramolecular Materials. *Chem. Rev.* **2016**, *116*, 962–1052. (b) Ma, Y. S.; Wang, C. H.; Zhao, Y. J.; Yu, Y.; Han, C. X.; Qiu, X. J.; Shi, Z. Perylene diimide dyes aggregates: optical properties and packing behavior in solution and solid state. *Supramol. Chem.* **2007**, *19*, 141–149.

(40) Haines, C.; Chen, M.; Ghiggino, K. P. The Effect of Perylene Diimide Aggregation on the Light Collection Efficiency of Luminescent Concentrators. *Sol. Energy Mater. Sol. Cells* **2012**, *105*, 287–292.

(41) Wang, X.; Zeng, T.; Nourrein, M.; Lai, B.-H.; Shen, K.; Wang, C.-L.; Sun, B.; Zhu, M. Concentration-dependent self-assembly structures of an amphiphilic perylene diimide with tri(ethyleneglycol) substituents at bay positions. *RSC Adv.* **2017**, *7*, 26074–26081.

(42) Feng, J.; Zhang, Y.; Zhao, C.; Li, R.; Xu, W.; Li, X.; Jiang, J. Cyclophanes of Perylene Tetracarboxylic Diimide with Different Substituents at Bay Positions. *Chem. – Eur. J.* **2008**, *14*, 7000–7010.

(43) Wang, J.; Zhan, X. Rylene Diimide Electron Acceptors for Organic Solar Cells. *Trends Chem.* **2019**, DOI: 10.1016/j.trechm.2019.05.002.

(44) Chen, H. Z.; Ling, M. M.; Mo, X.; Shi, M. M.; Wang, M.; Bao, Z. Air Stable n-Channel Organic Semiconductors for Thin Film Transistors Based on Fluorinated Derivatives of Perylene Diimides. *Chem. Mater.* **2007**, *19*, 816–824.

(45) Boobalan, G.; Imran, P. M.; Nagarajan, S. Self-Assembly, Optical, and Electrical Properties of a Novel Water-Soluble Perylene Bisimide. *J. Electron Mater.* **2011**, *40*, 2392–2397.

(46) Kumari, N.; Naqvi, S.; Kumar, R. Naphthalene diimide self assembled ribbons with high electrical conductivity and mobility without doping. *J. Mater. Sci.* **2018**, *53*, 4046–4055.

(47) Wu, N.; Zhang, Y.; Wang, C.; Slattum, P. M.; Yang, X.; Zang, L. Thermoactivated Electrical Conductivity in Perylene Diimide Nanofiber Materials. *J. Phys. Chem. Lett.* **2017**, *8*, 292–298.

(48) Wu, N.; Wang, C.; Bunes, B. R.; Zhang, Y.; Slattum, P. M.; Yang, X.; Zang, L. Chemical Self-Doping of Organic Nanoribbons for High Conductivity and Potential Application as Chemiresistive Sensor. *ACS Appl. Mater. Interfaces* **2016**, *8*, 12360–12368.

(49) Blakesley, J. C.; Castro, F. A.; Kylberg, W.; Dibb, G. F. A.; Arantes, C.; Valaski, R.; Cremona, M.; Kim, J. S.; Kim, J.-S. Towards reliable charge-mobility benchmark measurements for organic semiconductors. *Org. Electron.* **2014**, *15*, 1263–1272.

(50) (a) Naqvi, S.; Gupta, N.; Kumari, N.; Garg, J.; Kumar, R. Synthesis and charge transport properties of new methanofullerenes. *New J. Chem.* **2017**, *41*, 1933–1939. (b) Naqvi, S.; Vasistha, N.; Kumar, M.; Kumar, R. Electron transport and ultrafast spectroscopic studies of new methanofullerenes bearing a heteroatom in the exohedral chain. *New J. Chem.* **2019**, *43*, 15626–15635.

(51) Grimm, B.; Schornbaum, J.; Jasch, H.; Trukhina, O.; Wessendorf, F.; Hirsch, A.; Torres, T.; Guldi, D. M. Step-by-step self-assembled hybrids that feature control over energy and charge transfer. *PNAS* **2012**, *109*, 15565–15571.

(52) Cook, S.; Furube, A.; Katoh, R. Analysis of the excited states of regioregular polythiophene P3HT. *Energy Environ. Sci.* **2008**, *1*, 294–299.

(53) Holman, M.; Yan, P.; Adams, D.; Westenhoff, S.; Silva, C. Ultrafast Spectroscopy of the Solvent Dependence of Electron Transfer in a Perylene bisimide Dimer. *J. Phys. Chem. A* **2005**, *109*, 8548–8552.